Benedek Horváth

Eötvös Loránd University
Faculty of Natural Sciences

Physics MSc

Master Thesis

Electron Power Absorption Mode Transitions in Capacitively Coupled Radiofrequency Plasmas

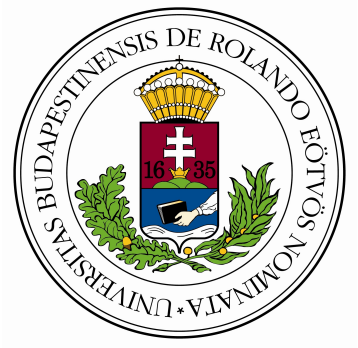

Scientific supervisor:

Dr. Aranka Derzsi

MTA Wigner RCP

Ins. for Sol. State Phys. and Optics

Supervisor at university:

Dr. Ákos Horváth

ELTE, Faculty of Natural Sciences

Department of Atomic Physics

May 2019

Contents

1 Introduction

Plasma Physics is a complex discipline, which is among the latest-evolved fields of Physics. For the description of plasmas, the laws of classical Electrodynamics, as well as Hydrodynamics, Statistical Physics and elementary atomic and molecular processes has to be considered. The study of low-temperature plasmas is an important field of plasma Physics because of their technological applications. They are basic tools in plasma processing applications, such as plasma based deposition, etching, sputtering and surface cleaning. Such systems are used for the production of various products, e.g. chips and solar cells [1]. Unlike thermal plasmas low-temperature plasmas are created and sustained by collisions of electrons with atoms of the background gas, the system having room temperature meanwhile. In capacitively coupled plasmas (CCPs) the plasma is excited by radiofrequency (RF) voltage (more details will be discussed later). In the current work CCPs operated in neon are studied via simulations and experiments. The thesis is structured in the following way: in the first chapter, the characteristics of a self-sustaining discharge via an example of a simple DC discharge are presented, followed by an introduction to the operation mechanisms of capacitively coupled radiofrequency discharges and the declaration of the objectives of the current study in details. In chapter 2, the simulation and the experimental method used in this work are described. In chapter 3 the simulation results in comparision with measurements are presented in detail, while in chapter 4 the conclusions are drawn.

1.1 Low-temperature gas discharges

For the overview of the operation of electrical gas discharges let us consider the DC glow discharge, the simplest plasma in laboratory. Let us take a DC power supply and connect it to a vacuum chamber via an ohmic resistor. The pressure of the discharge gas in the chamber has to be among 0.1 Pa and 10000 Pa, and the electrodes in the two edges of the chamber has to be made of conductive material (see figure 1 for a sketch

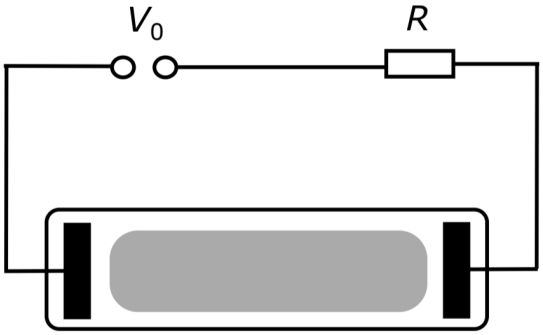

Figure 1: The sketch of the circuit of a DC glow discharge [2].

of the system). The simplest discharges to model are operated in noble gases, in which the vast majority of the charged particles are single-charge ions and electrons.

The basic mechanism of the glow discharge is breakdown of the gas. For breakdown, charged particles have to appear in the discharge cell which is filled with the neutral gas. Primary charged particles can originate from the (cosmic) background radiation, an X-ray source or can be emitted from the cathode by heating. Electrons and ions are accelerated by the electric field and they collide with the atoms of the background gas. Three different types of collision can occur: elastic scattering, atomic excitation and ionization. The latter has key importance in breakdown, as new charged particles are created in it. As more and more charged particles are accelerated in the system, collisions, as well as ionizations, occur more and more frequently. This multiplication of charged particles is called an electron avalanche[1].

The simplest model for breakdown is Townsend's theory. As a result of an avalanche in a DC cell, electrons arrive at the anode, while ions arrive at the cathode. A certain portion of the ions hitting the cathode induce the emission of new electrons from it. According to Townsend's model, the criterion of breakdown is that the ions produced

[1]Note that gaseous particle detectors widely used in particle and nuclear Physics operate based on this process. The primary charge is the particle to detect, which causes an avalanche and can be measured as a pulse in the circuit.

in an avalanche have to induce the emission of one new electrode from the cathode on average. With this criterion fulfilled, space charges appear in the system and modify the electric field, allowing the development of a stationary state within a wide parameter regime through feedback mechanisms.

In a stationary discharge charge reproduction is continuous in the gas phase and at the electrode surfaces (in the case of the DC discharge at the surface of the cathode). In the gas phase the basic mechanism for charge reproduction is ionization induced by electrons, while at the electrodes it is ion-induced secondary electron emission. In addition to ionization, elastic scattering of electron on atom and electron-induced atomic excitation also have key importance in forming the discharge properties. Besides electrons, ions can also collide with the atoms of the background gas either elastically or causing ionization (the latter is only remarkable at high voltage). All the above collision processes have energy-dependent cross sections, for which data are available in the literature. The cross sections of each process and their relation to each other determine the frequency of ionization and consequently the discharge characteristics together.

1.2 Capacitively coupled plasmas (CCPs)

CCP is a type of low-temperature discharge, in which the plasma is excited by RF voltage. The frequency typically ranges from 1 MHz to 100 MHz. The waveform is usually sinusoidal, however, higher harmonics of a sinusoidal component are often used to form multifrequency waveforms with various non-sinusoidal shapes. In the current work, only single-frequency sinusoidal RF discharges are studied. The pressure can be set within a wide range starting from 0.1 Pa up to atmospheric pressure. The most important part of the system is a vacuum chamber with two plane-parallel electrodes, in an arrangement similar to a capacitor (see figure 2). That is why it is often referred to as capacitively coupled RF discharge. One of the electrodes is grounded, while the other one is driven by RF voltage. The generator and the powered electrode is connected via a linear power amplifier and an impedance matching box, i.e. an RLC

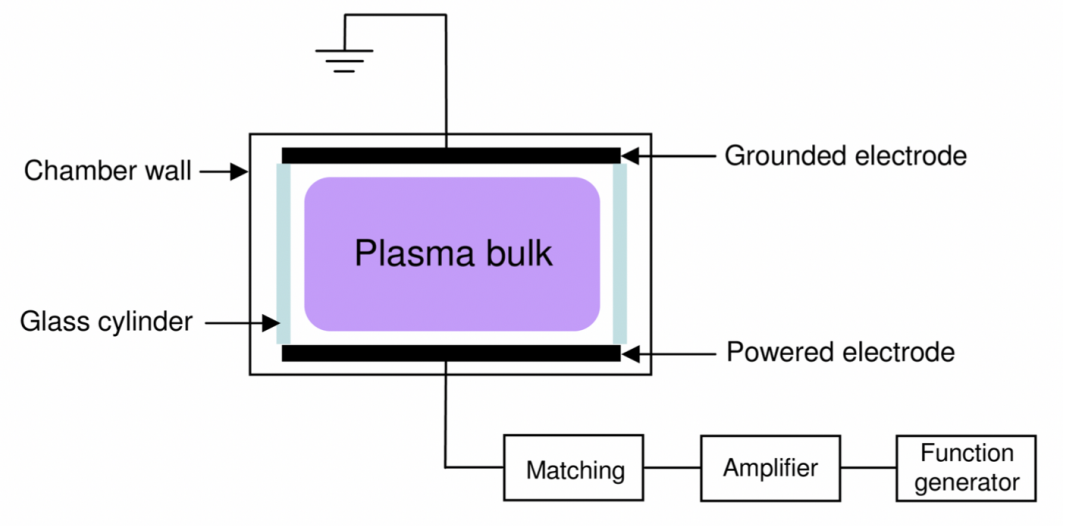

Figure 2: Sketch of the circuit of a CCP.

unit that tunes the impedance of the circuit in order to maximize the power delivered to the plasma. Given that the diameter of the electrodes is significantly larger than the distance between them, the current flows approximately perpendicular to the planes of the electrodes in the plasma.

As for a CCP in operation, it remarkably differs from a DC discharge. One crucial property is that no secondary electrons emitted from the electrode material are needed for the self-sustainment of the plasma. Another important characteristic of a CCP is that it can be operated between electodes made of an insulator. This feature make them widely applicable in industry: with appropriate control of the flux and energy of ions at the electrodes such discharges can be used for the modification of surfaces that are used as electrodes.

In figure 3 the spatio-temporal distribution of the electric field (panel (a)), the ion density (panel (b)) and the electron density (panel (c)) are shown in the discharge gap for an RF discharge operated in argon, driven by the voltage waveform

$$\Phi(t) = V_0 \cos(2\pi f t), \tag{1}$$

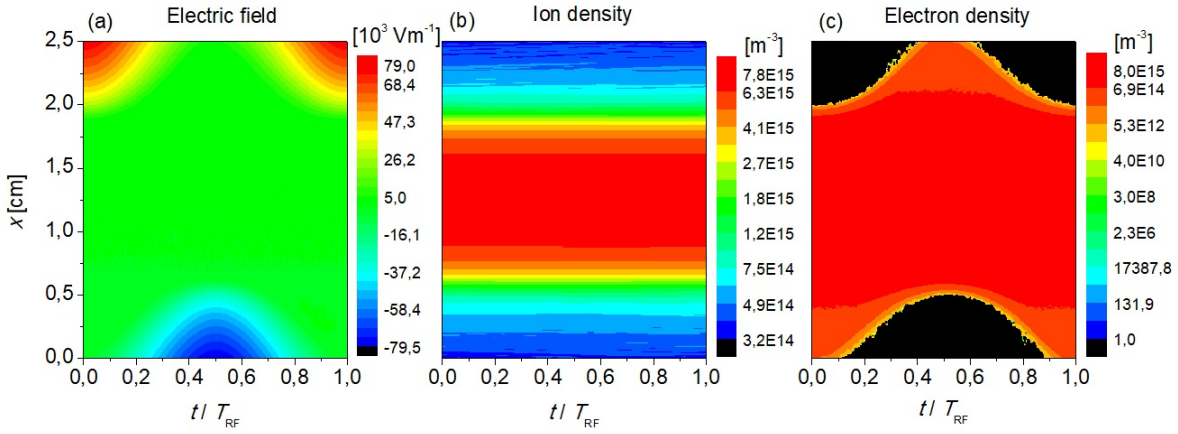

Figure 3: Spatio-temporal plots of (a) the electric field, (b) the ion density and (c) the electron density. The horizontal axis corresponds to one RF period. On the vertical axis, $x = 0$ cm corresponds to the powered, while $x = 2.5$ cm to the grounded electrode. The contour scale is linear in panel (a) and logarithmic in panels (b) and (c). Discharge conditions: Ar gas, $V_0 = 300$ V, $f = 13.56$ MHz, $L = 2.5$ cm, $p = 10$ Pa. (The figure was created by PIC/MCC simulation, a method to be introduced in chapter 2.1.)

where $f = 13.56$ MHz is the frequency of the driving voltage and $V_0 = 300$ V is its amplitude. The distance between the electrodes is $L = 2.5$ cm and the pressure is $p = 10$ Pa. In the spatio-temporal plots, time is shown on the horizontal axis and its range corresponds to one RF period. The vertical axis shows the spatial coordinate, with $x = 0$ cm corresponding to the powered electrode (at the bottom) and $x = 1.5$ cm to the grounded electrode (at the top). As it can be seen in the distribution of the electric field, charged particles make the system strongly nonlinear. The electric field is concentrated near the electrodes, where it follows the oscillation of the driving voltage, while the value of the electric field is close to zero inside, as a result of shielding. At the typical RF frequency range the electrons follow the oscillation of the RF modulated electric field, while the ions move according to its space average due to their higher mass. As a result, the density profile of the ions becomes stationary, while the regions near the electrodes change between states saturated and evacuated by electrons. These RF

modulated regions at the boundary of the plasma are called sheaths, while the region between them is called bulk. The density of the ions and the electrons is maximal in the middle of the chamber, and it decreases towards the electrodes in both directions. The bulk region forms a quasi-neutral plasma, where the density of ions and electrons is technically equal and stationary. The ion density profile is symmetric in the whole chamber, while the drop points of the electron density change dynamically. The sheath length changes as a function of time within the RF period at both electrodes. When the driving voltage is maximal (at $t/T_{RF} = 0.5$), the sheath length is minimal at the powered electrode and maximal at the grounded one. Half an RF period later, the situation gets reversed. At the phase of sheath expansion ($0 < t/T_{RF} < 0.5$ at the powered electrode, i.e. the bottom of figure 3) the electrons gain energy from the high electric field that accelerates them away from the electrode [1]. This periodic expansion of the sheaths is a crucial phenomenon in terms of the energy absorption of the system, making the RF plasma self-sustaining. As a coupled effect of the sheath expansion and the ionization caused by the electrons accelerated at that phase, the energy absorption of the total electron population is positive on average for a RF period. Electrons with high energy provide the continuous supply of the system with charged particles via ionization. As a result, the discharge can become self-sustaining due to gas-phase processes, and surface processes are not essential in maintaining the discharge. This is a remarkable difference in comparison with a DC discharge, in which the secondary electrons escaping from the cathode are essential in the charge supply of the system.

The above energy-absorption mechanism happening at the phase of sheath expansion is called α-mode, because of the intensive ionization caused by the accelerated electrons, which is connected to Townsend's α coefficient for ionization[2]. In addition to this mechanism, the so-called γ-mode can also become significant in the power absorption. In this case secondary electrons originating from the electrodes upon ion impact

[2]Townsend's α coefficient describes the efficiency of ionization in the gas phase: it is the number of electron-ion pairs created by one electron per unit distance.

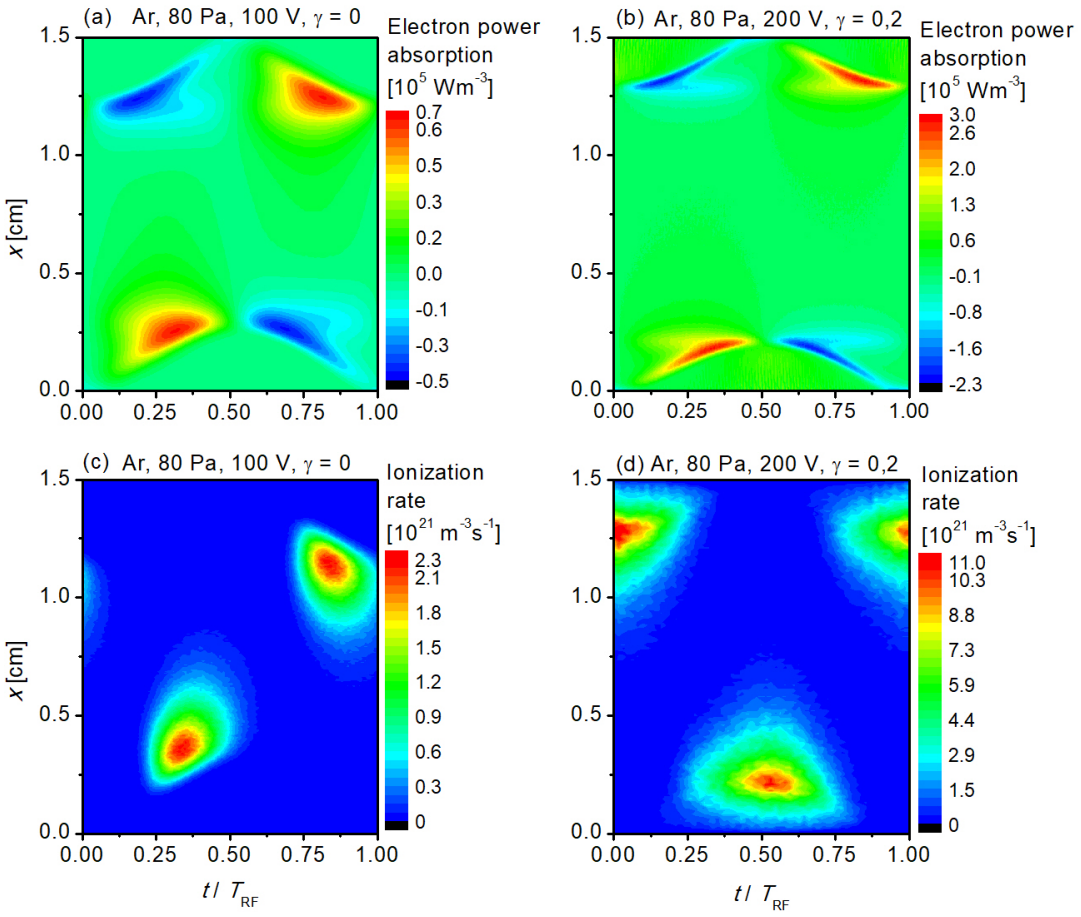

Figure 4: The spatio-temporal plot of the power absorption of the electrons (a, b) and the ionization rate (c, d) in α-mode (a, c) and γ-mode (b, d) discharge operation [3]. Discharge conditions: Ar gas, $f = 13.56$ MHz, $L = 1.5$ cm. Other parameters are shown in the panels. The position of the powered electrode is at $x = 0$ cm, while the grounded one is at $x = 1.5$ cm. (The figure was created by PIC/MCC simulation, a method to be introduced in chapter 2.1.)

play an important role in maintaining the discharge. These electrons are usually called γ electrons, after the γ secondary electron emission coefficient. The two different operation modes are demonstrated in figure 4 [3], showing the spatio-temporal plot of the power absorption of the electrons (top row) and the ionization rate, i.e. the number of ionizations per unit time per unit volume (bottom row). The power absorption of electrons are similar in the two operation modes (figure 4(a, b)), as this quantity shows an average for the whole population of electrons. However, ionization and excitation processes are caused by high-energy electrons, whose number is a small portion of all electrons. The ionization patterns show essential differences between the two modes. In α-mode (4(c), $\gamma = 0$) ionization is concentrated at the phase of sheath expansion and takes place in the bulk region. In γ-mode, the electrons escaping from the electrodes are strongly accelerated in the expanded sheath by the high electric field, causing intensive ionization within the sheaths (4(d). The latter dynamics dominates the discharge operation in case of low electron free path, high electric field within the sheaths and efficient surface processes.

In the discussion above several plasma parameters were mentioned (electric field, ion and electron density, ionization rate, electron power absorption). Note that the driving force of all these quantities is the RF exciting voltage and the condition it raises for the particle current: no DC current can flow in the circuit. As the wiring is serial, this condition needs to be satisfied in the plasma as well. In other words, the condition means that the current has to be zero on time average for a RF period (T_{RF}). Given there are single positive ions and electrons in the system, the criterion can only be fulfilled if the ion and electron fluxes are equal at both electrodes during an RF period:

$$\langle \Gamma_i \rangle_{T_{\mathrm{RF}}} = \langle \Gamma_e \rangle_{T_{\mathrm{RF}}}. \tag{2}$$

1.3 Objectives

The aim of this work is to study the electron power absorption modes of RF discharges operated in neon and to provide a detailed comparative study of simulations and experiments in a wide parameter regime. Phase-resolved optical emission spectroscopy (PROES) is a powerful technique for the spatio-temporal observation of the optical emission of plasmas, based on which the population density of a certain atomic excited state can be studied experimentally. With the appropriate choice of a high-energy emission line, one can gain insight into the dynamics of high-energy plasma particles. As ionization, the fundamental process regarding the discharge operation, is caused by high-energy particles, PROES is often applied for the indirect experimental study of the ionization dynamics in CCPs. However, simulations show that the ionization dynamics can be remarkably different from the excitation dynamics in several cases, especially when a high number of secondary electrons are generated at the electrodes, gain high energies of hundreds of eV and induce significant ionization in the sheaths [4]. Since the cross section of electron impact ionization in neon is approximately one or two orders of magnitude higher in the high-energy regime (above 50 eV, see later in figure 7) than the cross sections of the various types of excitations, the spatio-temporal distribution of the excitation observable by PROES can show a significantly different picture from the ionization dynamics. For several reasons to be discussed in chapter 2.2.2, the 2p1 line of neon is an appropriate level to be measured by PROES, and it is widely used for the spectroscopy of RF discharges operated in different gases and gas mixtures, by adding neon as trace gas to the background gas in a low concentration. In the current research CCPs operated in pure neon are studied. The use of pure neon allows a detailed comparison of the excitation and ionization dynamics obtained from experiments and simulations under exactly the same discharge conditions for a system in which the main discharge gas is the same as the trace gas for PROES. This way the inaccuracy factor resulting from the interaction of the trace gas with the discharge gas (usually neglected in the simulations) is excluded. Neon discharges are studied here in

a wide range of the driving frequency, the pressure and the voltage amplitude, allowing the study of the dependence of the electron power absorption and ionization modes on these operation parameters. This study aims to reveal the applicability of PROES (which provides the spatio-temporal distribution of the excitation dynamics) to probe the discharge operation mode (which is determined by the spatio-temporal distribution of the ionization dynamics).

2 Materials and methods

2.1 Simulation method

The simulation method used in this work is the so-called Particle-in-Cell/Monte Carlo Collisions (PIC/MCC) simulation, which is a widely used particle-based kinetic approach to the description of low-pressure CCPs [5]. In the PIC approach there are two important simplifications.

1. Instead of tracing individual particles, superparticles are traced, which represent groups of particles whose coordinates are moved together.

2. Instead of pairwise interactions of the charged particles, meanfield approximation is used for the calculation of the electrostatic interactions.

These are complemented with a Monte Carlo type modelling of the particle collisions. The PIC/MCC simulation code used in this work is one dimensional in space and three dimensional in velocity space (1d3v). This is suitable to describe CCPs with cylindrical symmetry. It means that the position of particles is only considered as a distance from the electrodes, since the plane-parallel setup has a cylindrical symmetry, making other directions irrelevant. Thus, all the plasma parameters are calculated in 1D. To be precise, this approach assumes that the area of the electrodes is infinite, which is a reasonable approximation when the diameter of the electrodes is much larger than the

distance between them. However, the consideration of velocities in 3D is important, since all velocity coordinates can change in collisions. In the simulations performed in the current study, the particles traced are Ne^+ ions and electrons. The time evolution of the RF discharge in followed in discrete timesteps in the simulation, and the Δt step has to be orders of magnitude smaller than the T_{RF} period of the RF driving voltage. In the simulations executed for this study the number of timesteps per RF cycle ranges from 5×10^3 to 2×10^5, depending on the driving frequency and other discharge conditions.

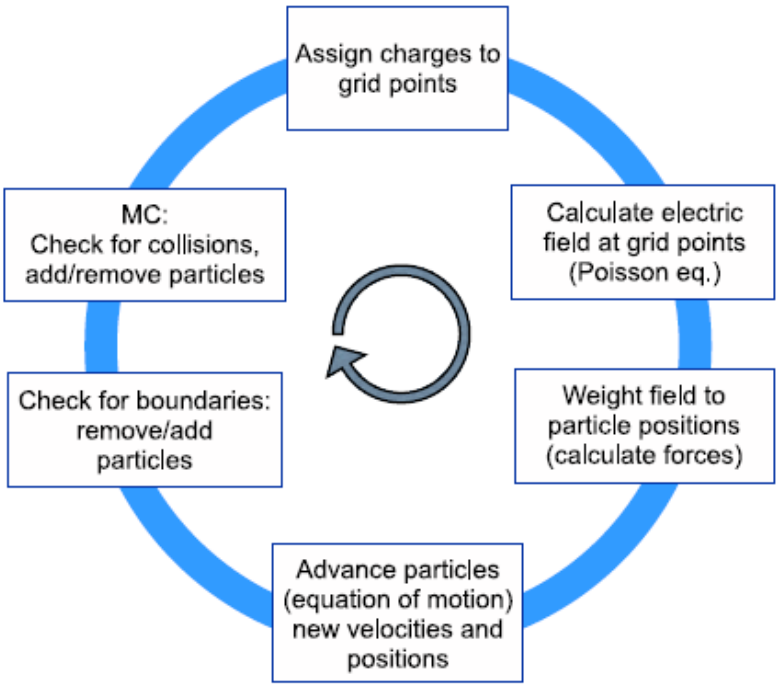

Figure 5: Flow chart of a PIC/MCC cycle carried out in each Δt timestep [6].

In figure 5 the flow chart of one PIC/MCC simulation cycle (performed in each Δt timestep) can be seen. The major steps are the following [6, 7, 8, 9]:

1. Assign the charges of superparticles to the points of a predefined computational grid.

2. Calculate the electrostatic potential and the electric field by solving Poisson equation on the grid. Input data are the value of the potential at the powered and the

grounded electrodes and the space charge.

3. Calculate the electric field at particle positions by linear interpolation and calculate the force acting on particles.

4. Integrate the equation of motion of each particle: calculate new positions and velocities.

5. Model surface processes: particles hitting the electrodes can be absorbed, reflected or they can induce secondary electron emission. (Side walls of the chamber are not considered in a 1D simulation.)

6. Model gas-phase processes, i.e. the collision of charged particles with the background gas by a Monte Carlo approach. The velocities of colliding particles are changed according to the type of collision, and coordinates are assigned to newly-created particles.

At the beginning of a simulation, superparticles and a grid is defined. The former means that a weight factor is set, which gives the number of charged particles to be traced together. In the current work this factor ranges from 10^3–10^6, always set in a way that the number of Ne^+ ion and electron superparticles would be around 10^5, providing an efficient modelling of discharges within reasonable runtime. The setup of the grid means that the chamber is divided into cells. In the simulations presented in this thesis the number of cells is between 200 and 300. A demonstration can be seen about the superparticles and the grid in figure 6. In each simulation cycle, the charge of each superparticle is assigned to the two grid points being closest to it. The charge is devided between the two grid points inversely proportional to their distance. This step results in a charge density concentrated at the points of the 1D grid, which makes the Poisson equation easy to solve. The boundary conditions come from the driving voltage at the electrodes, i.e. constantly zero potential is assumed at the grounded electrode and the voltage of the RF generator at the certain timestep is applied to the

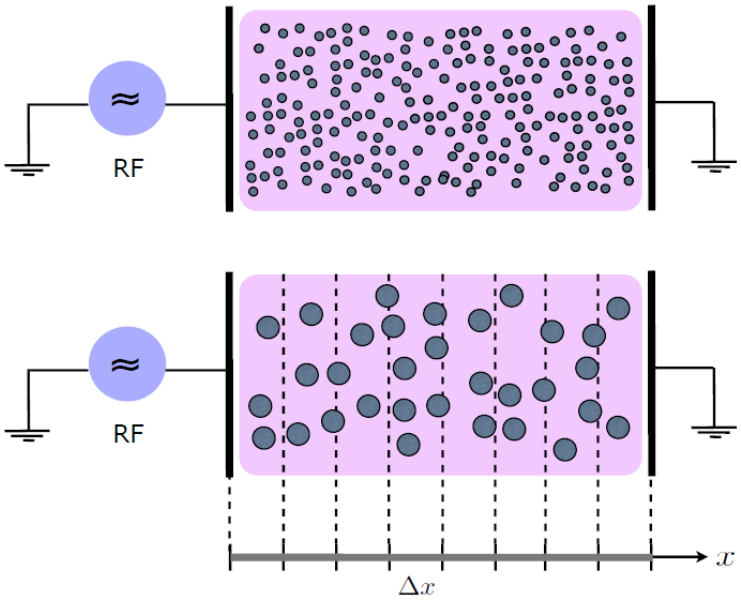

Figure 6: PIC simplifications: consideration of superparticles and assignment of a computational grid [10].

powered electrode. As a solution of the Poisson equation one can get the electrostatic potential at the grid points, from which the electric field is calculated at the grid points by numeric derivation. After that the electric field is calculated at particle positions by linear interpolation, from which the electrostatic force acting on particles and finally the equations of motion can be specified. The numeric integration of Newton's equations is performed by the leapfrog scheme, i.e. the timestep is the same for the coordinates, velocities and forces, however, the velocity is evaluated with half timestep shift with respect to the other two quantities. Precisely:

$$v\left(t+\frac{\Delta t}{2}\right) = v\left(t-\frac{\Delta t}{2}\right) + \frac{q}{m}E(x(t))\Delta t, \tag{3}$$

$$x(t+\Delta t) = x(t) + v\left(t+\frac{\Delta t}{2}\right)\Delta t,$$

where q and m is the charge and mass of the superparticle and $E(x(t))$ is the electric

field at the position of the particle.

The surface processes taken into account are electron reflection and secondary electron emission (SEE) induced by ions. They are described in a simplified way in the present PIC/MCC simulations, i.e. constant surface coefficients are specified as input parameters. Since the aim of this work is to simulate a certain experimental setup, i.e. a geometrically symmetric CCP reactor with electrodes made of stainless steel (as it will be described in detail in section 2.2.1), the assumptions for the surface coefficients need to reflect the properties of a stainless steel surface. In case of the electrons hitting the electrode surface, a constant probability of $\delta_e = 0.2$ is assumed for elastic electron reflection, as it is often set in PIC/MCC simulations of CCPs [11]. This means that 20 % of the electrons hitting the electrodes are reflected mirror-like, without loss of energy. All the other electrons are absorbed by the electrodes. The outcome of each electron-surface collision is decided by a Monte Carlo approach: a random number is drawn from a uniform distribution between 0 and 1 (R_{01}). The electron is reflected if $R_{01} < \delta_e$, otherwise it is absorbed. As for the treatment of the interaction of Ne^+ ions with the electrodes, a constant secondary electron emission (SEE) coefficient, γ is assumed. In this work, $\gamma = 0.2$ is set in most of the simulations, however, some calculations are performed with γ values of 0.3 and 0.4, in order to demonstrate the effects of ion-induced secondary electrons (γ-electrons) on the discharge characteristics. The simulation results obtained by using different γ coefficients are compared to the measured data.

The modelling of the collision processes in the simulation is a complex task [12], taking a remarkable portion of simulation time together with the integration of the equations of motion. In the plasma ions and electrons collide with atoms of the background gas (which are not traced in the simulation, they are only considered by a constant gas density according to the gas pressure). Within Δt timestep the probability for a given charged particle to collide with an atom is

$$P_c(\Delta t) = 1 - e^{-n_0 \sigma(g) g \Delta t}, \tag{4}$$

where n_0 is the density of the background gas, σ is the total cross section taking all collision processes into account, and g is the relative velocity of the particle with respect to the atom it potentially collides with. The simulation timestep has to be small enough so that the probability of more than one collision for the same particle within one timestep would remain negligible. The occurance of a collision is decided in a similar way as described in the case of surface processes: the collision happens if a random number $R_{01} < P_c$. The type of collision is chosen according to the ratio of the cross sections of the various collision processes, with the use of another random number. When a collision takes place, the velocity vector of the particle changes. The transformation is performed according to the energy and angular distribution of the certain type of collision, in the center of mass frame. Note that in electron-atom collisions the atom is considered to be at rest (cold-gas approximation), while in ion-atom collisions the velocity of the atom is drawn from a random Maxwellian sample.

The cross sections of the collision processes taken into account in the PIC/MCC simulation of neon RF discharges [13, 14] are shown in figure 7. For the collision of Ne^+ ions with Ne atoms, isotropic and backward elastic scattering is considered (the latter means elastic scattering with angle of π). The term elastic means that the kinetic energy of the ion is conserved. For the collision of electrons with Ne atoms, elastic scattering, excitation and ionization is considered. 7 possible atomic excitation processes are taken into account with different cross sections. Among them there is a special process, the Ne 2p1 excitation, i.e. the state whose population dynamics is observed experimentally by PROES. Its cross section was taken from the Biagi-v7.1 dataset [14], while the other ones were obtained from the SIGLO dataset [13], which did not contain the Ne 2p1 excitation separately. The excitation of the Ne 2p1 line is only included in the simulation as diagnostics. This way the spatio-temporal distribution of the Ne 2p1 excitation is obtained in relative units, just like the PROES measurement results.

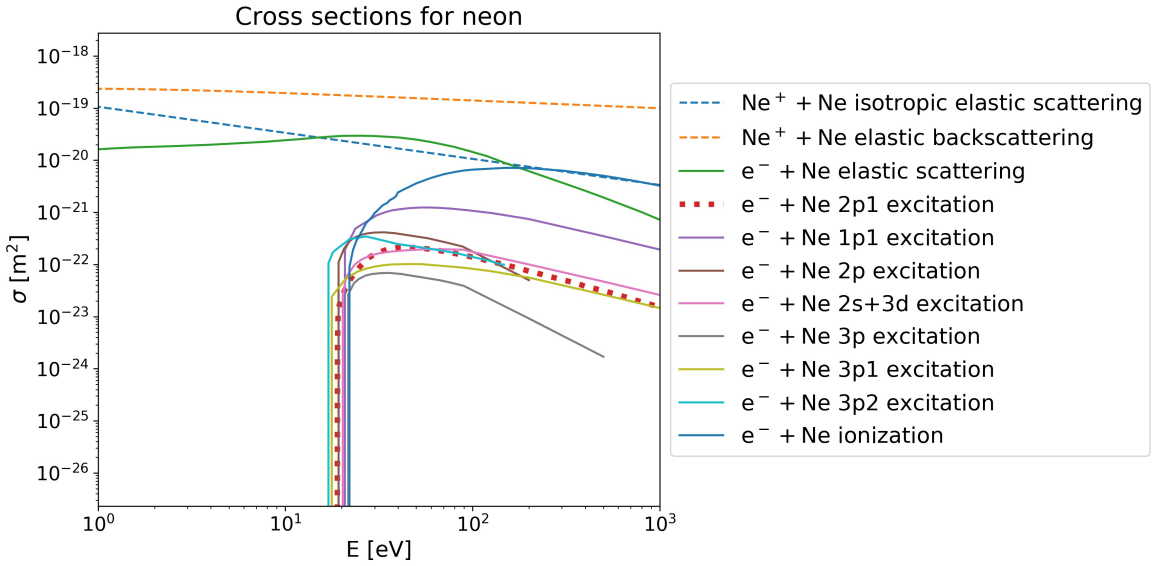

Figure 7: The cross sections of the different types of collisions considered in the PIC/MCC simulations of neon, as a function of the kinetic energy in the center of mass frame. The dashed lines (the first two lines in the legend) correspond to ion-atom collisions, while the continuous lines correspond to electron-atom collisions. The thick dotted red line corresponds to the Ne 2p1 excitation, which is only included in the diagnostics.

2.2 Experimental method

For the experimental study of the optical emission of CCPs space and time resolved, phase resolved optical emission spectroscopy (PROES) technique is used on a geometrically symmetric CCP source. In section 2.2.1, the setup used for the measurements is introduced in detail, while section 2.2.2 contains a detailed theoretical overview on the method of PROES.

2.2.1 Laboratory setup

A detailed sketch of the experimental setup is shown in figure 8. The electrodes are located in a vacuum quartz cylinder, which contains low-pressure pure neon gas. The

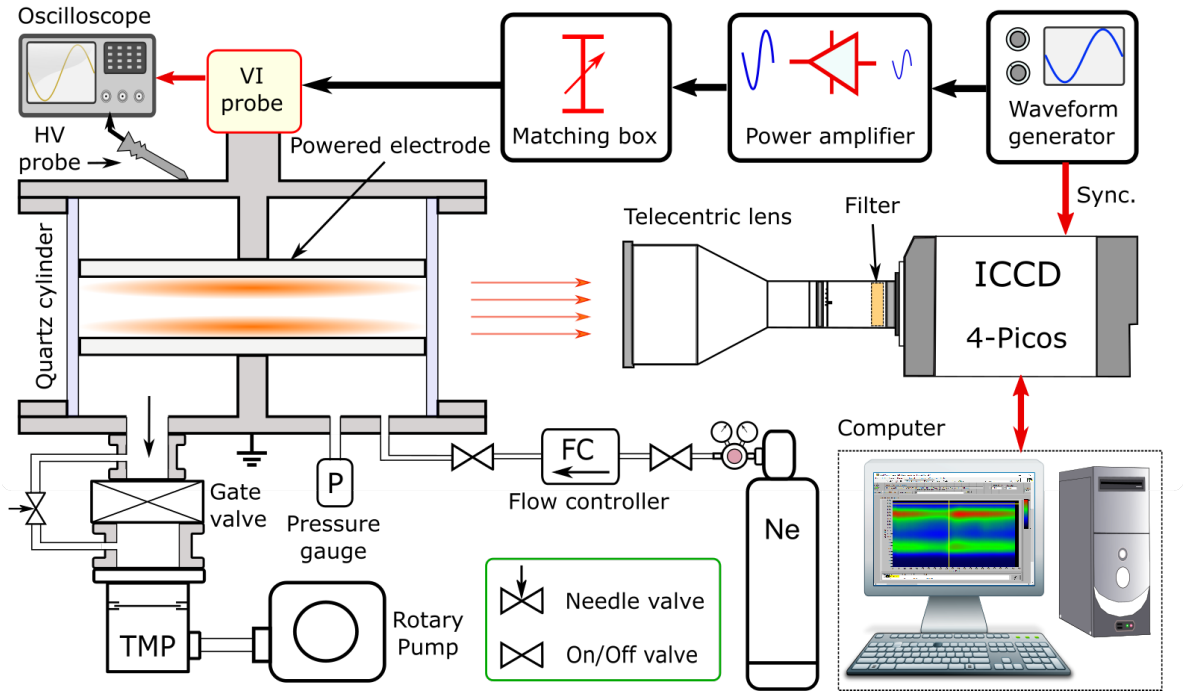

Figure 8: Detailed sketch of the experimental setup: symmetric CCP with ICCD camera.

chamber can be evacuated when the gate valve is open, with a turbomolecular and a rotation pump. A needle valve allows fine control of the gas pressure in the chamber. In the current study, the gas pressure ranges from 60 Pa to 500 Pa. The measurements are performed in gas flow of about 3 sccm (the standard condition meaning 1 bar and 0 $^{\circ}C$) tuned with a flow controller, in order to keep the purity of the neon gas in the chamber. The gas supply can be halted with two on/off valves designed for high and low pressure, respectively. The stainless steel electrodes are plain-parallel and orbicular with identical diameters of 14.2 cm, while the gap between them is 2.5 cm. The upper electrode is the powered one, driven by the RF waveform generator (Juntek JDS-2900),

to which it is connected via a linear power amplifier (RM BLA-300) and an impedance matching box (MFJ-949E), i.e. an RLC unit that tunes the impedance of the circuit in order to maximize the power delivered to the plasma. The lower electrode is grounded. The frequency of the driving voltage is varied between 1.70 and 13.56 MHz, while its peak-to-peak value (double of the amplitude) is changed between 300 and 425 V.

The main diagnostic tool of the setup is a fast-gateable ICCD camera (4 Picos from Stanford Computer Optics), with which the Ne 2p1 state with wavelength of 585.25 nm is measured space and time resolved in the discharge. In order to limit the signal to the proper wavelength an interference filter with bandwidth 585 ± 5 nm is used. The principle of a PROES measurement is demonstrated in figure 9. The electric controller of the camera receives a trigger signal from the waveform generator synchronized with the RF frequency driving the plasma, after which the controller puts in a certain delay. The delay determines which phase of the RF period is scanned by the camera. The collection of photons lasts for the time of a narrow gatewidth varying from 2 to 8 ns in the current study, while the length of the RF period varies between 73.7 and 588 ns. One phase of the RF period is scanned from 10^4 to 10^6 times (depending on the emission of the plasma), and each phase is scanned uniformly. The time required for one measurement is determined by the repetition rate of the camera, i.e. the number of short scans manageable per unit time, which is approximately 200 kHz, typically requiring a couple of minutes to perform one phase-resolved measurement. The spatial resolution is determined by the number of pixels in the camera sensor: the 170 pixels result in a resolution of approximately 150 μm. The camera has a telecentric lense (Thorlabs MVTC23013 0.128x bi-telecentric lense), with which 2D pictures can be produced. As in a symmetric CCP only the position in the discharge axis (the direction perpendicular to the electrodes, i.e. vertical in the current setup) matters, the pictures are integrated in horizontal direction, which reduces noise remarkably.

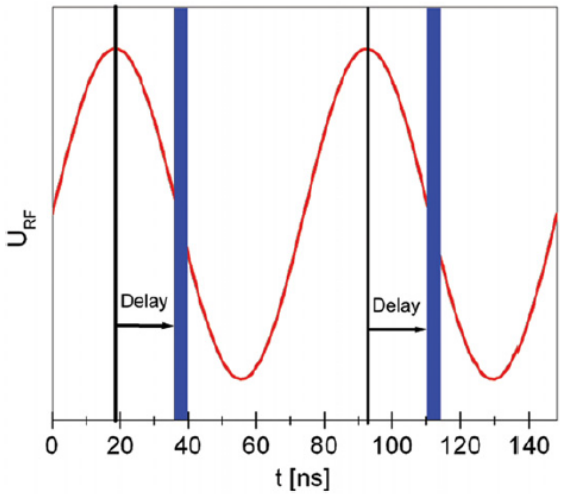

Figure 9: Operation of PROES: the trigger signals at the peak of each RF period, the delay after which the camera begins the collection of photons and the time slots of collection. The discharge frequency is $f = 13.56$ MHz and the gatewidth is 4 ns in the current setup [15].

2.2.2 Theoretical background

The theoretical consideration behind PROES is based on population dynamics: the method operates with the time-dependent measurement of the population density of a specifically chosen excited rare gas state, as introduced in [15]. The basic concept of the measurement is that the spatio-temporal excitation rate, $E_{0,i}(x,t)$, i.e. the frequency of electron impact excitation from the ground state to the observed level i per unit volume, can be calculated from the measured spatio-temporal emission. The rate equation of the excited state i with population density n_i is:

$$\frac{dn_i(x,t)}{dt} = n_0 E_{0,i}(x,t) + \sum_m n_m E_{m,i}(x,t) + \sum_c W_{ci} n_c(x,t) - \lambda_i n_i(x,t). \qquad (5)$$

The first term represents excitation from the ground state to level i, with n_0 meaning the population density of the ground state. The term $\sum_m n_m E_{m,i}(x,t)$ considers excitation from metastable levels with population densities n_m, while $\sum_c W_{ci} n_c(x,t)$ represents

cascades from higher levels c with population densities n_c to state i with transition probabilities W_{ci}. The last term considers the decay of state i, where λ_i is an effective decay rate:

$$\lambda_i = \sum_k W_{ik} g_{ik} + \sum_q C_q n_q, \tag{6}$$

Here two kinds of decays are taken into account: $\sum_k W_{ik} g_{ik}$ represents transitions to other states via photon emission without reabsorption of the photon (W_{ik} being the transition probability and g_{ik} being the probability that the emitted photon is not absorbed), and $\sum_q C_q n_q$ represents quenching, i.e. collisional de-excitation without radiation, where n_q is the density of collision partner of type q and C_q is the corresponding quenching coefficient (probability per unit time). Reabsorption of radiation is an effect that decreases the decay rate and increases the lifetime, and it is remarkable in the case of the overpopulated ground state: $g_{i0} \approx 0$, i.e. practically each irradiated photon is reabsorbed in case of de-excitations to the ground state, making zero contribution to the effective decay rate. In a quenching process the energy lost in de-excitation is transferred into the kinetic energy of the two colliding particles, thus the process increases the decay rate. The rate equation above (5) is a part of a system of coupled differential equations together with the rate equations for all metastable and cascade levels containing several unknown quantities, e.g. quenching coefficients, making the $E_{0,i}(x,t)$ excitation rate from the ground state to a certain level i difficult to calculate. However, several simplifications can be made with the proper choice of the observed excited level. In an optimal case, the effect of cascades, metastables and quenching can be neglected, making equation (5) much simpler:

$$E_{0,i}(x,t) = \frac{1}{W_{i0} n_0} \left(\frac{dn_i'(x,t)}{dt} + \lambda_i n_i'(x,t) \right), \tag{7}$$

with

$$n_i'(x,t) = W_{i0} n_i(x,t), \tag{8}$$

where W_{i0} is the transition probability from level i to the ground state, and $n_i'(x,t)$ represents the emitted number of photons per unit volume and time, resulting from that type of transition. PROES is based on the time-dependent detecting of these photons in each pixel of the camera. In each time window t_k, the 2D spatial emission is measured, which is then integrated in the spatial direction parallel to the electrodes, resulting in a 1D emission picture proportional to the value of the spatio-temporal emission at time t_k, $n_i'(x,t_k)$, where x means the direction perpendicular to the electrodes. Finally, with the use of equation (7), a quantity proportional to the $E_{0,i}(x,t)$ spatio-temporal excitation rate can be obtained. Note that the population density of the ground state, n_0 is unknown, however, its value is irrelevant in calculating the excitation rate in relative units.

In order to perform a valuable PROES measurement on a CCP, several conditions need to be satisfied, in accordance with the above [15]:

1. The optical transition rates of the gas need to be known (see equations (6)–(8), in which the transition probabilities are variables).

2. Excited population due to cascades, excitation from metastable levels and quenching need to be negligibly low.

3. Enough intensity of the measured emission line is necessary, and no superposition with other lines is required.

4. The lifetime of the measured line has to be short enough to temporally resolve the RF period (the shortest period being 74 ns here).

One energy level that satisfies these criteria well in neon gas is Ne 2p1 with lifetime of 16.26 ns and threshold energy for electron impact excitation from the ground state

of 18.965 eV [16]. Given that this is an excited state with high energy, metastables cannot contribute to it (their excitation energy being 16.6 eV), and the contribution of cascades from higher energies to the population of this level is also particularly low [17], while quenching is negligible at the low-pressure regime studied here.

3 Results and discussion

In this section, the results of PROES measurements and PIC/MCC simulations are compared for a wide parameter regime. The pressure ranges from 60 Pa to 500 Pa and the frequency of the driving voltage is varied between 1.70 MHz and 13.65 MHz. The peak-to-peak value of the driving voltage, V_{pp}, i.e. the double of the voltage amplitude ($V_{\mathrm{pp}} = 2V_0$), is varied between 300 V and 425 V. The ion-induced SEE coefficient, γ is set to 0.2 in most cases. Exceptions will be specified below. The results are shown in the order of increasing frequency, i.e. 1.70 MHz (figure 10), 3.39 MHz (figure 12), 6.78 MHz (figure 13) and 13.56 MHz (figure 14), respectively. Each figure, in the first row, contains the spatio-temporal plots of the Ne 2p1 excitation rate obtained by PROES measurements, while the PIC/MCC simulation results on the excitation rates and the ionization rates are shown in the second and third rows, respectively, for the same discharge conditions. In the spatio-temporal plots of the discharge characteristics shown in figures 10-14 the horizontal axis corresponds to one RF period, and the vertical axis corresponds to the distance from the powered electrode in electrode gap units, i.e. the whole discharge cell is mapped, with $x/L = 0$ being the position of the powered electrode and $x/L = 1$ being the position of the grounded one. The time-dependent data collection in the case of PROES measurements has already been discussed in chapter 2.2.2. In the PIC simulations, the elementary excitation and ionization collisions are counted in a space and time dependent way through several thousands of RF cycles, and the results are averaged to one RF cycle. The sheath edge positions obtained from the simulations are shown as white lines in the simulation plots. The position of the

sheath is calculated by a criterion proposed by Brinkmann [18]:

$$\int_0^s n_e(x)dx = \int_s^{L/2} (n_i(x) - n_e(x))dx, \tag{9}$$

where s is the distance of the sheath from the nearest electrode, L is the electrode gap, n_e and n_i are the electron and ion densities.

3.1 Fixed pressure

Figure 10 contains data for 1.70 MHz driving frequency and a relatively high fixed pressure of 500 Pa, and it demonstrates the effects of varying the peak-to-peak voltage between 300 V and 425 V, one certain value corresponding to a column of the figure. In the spatio-temporal distribution of the Ne 2p1 excitation rate measured by PROES (first row), a transition from α- to γ-mode is suggested, as the peak-to-peak voltage is increased. More precisely, at lower peak-to-peak voltages, excitations caused by high-energy electrons are mostly observed in the phase of sheath expansion. At higher peak-to-peak voltages, though, electrons cause excitation mostly within the sheaths, while it is expanded. In the second row, the excitation rate obtained from PIC/MCC simulation is shown, i.e. the same quantity as in the first row. Although the tendency of transition from α- to γ-mode is visible in the simulated series of data as well, it suggests different picture of the excitation than the measurement, for most values of the peak-to-peak voltage. Namely, the γ peak is more intensive in the measured data than in the simulated excitation. This can be a consequence of inaccuracy of the $\gamma = 0.2$ SEE coefficient in the simulation for this low frequency of 1.70 MHz, as secondary electrons can have a crucial role in the excitation and ionization dynamics. Generally, in case of high sheath potential, the secondary electrons escaping from the electrodes are intensively accelerated, and most of them collide with the atoms of the background gas.As for the ionization calculated by PIC/MCC simulation (see the third row), its spatio-temporal distribution differs from both the measured and the simulated excitation rate for most values of the peak-to-peak voltage, i.e. the γ peak seems less

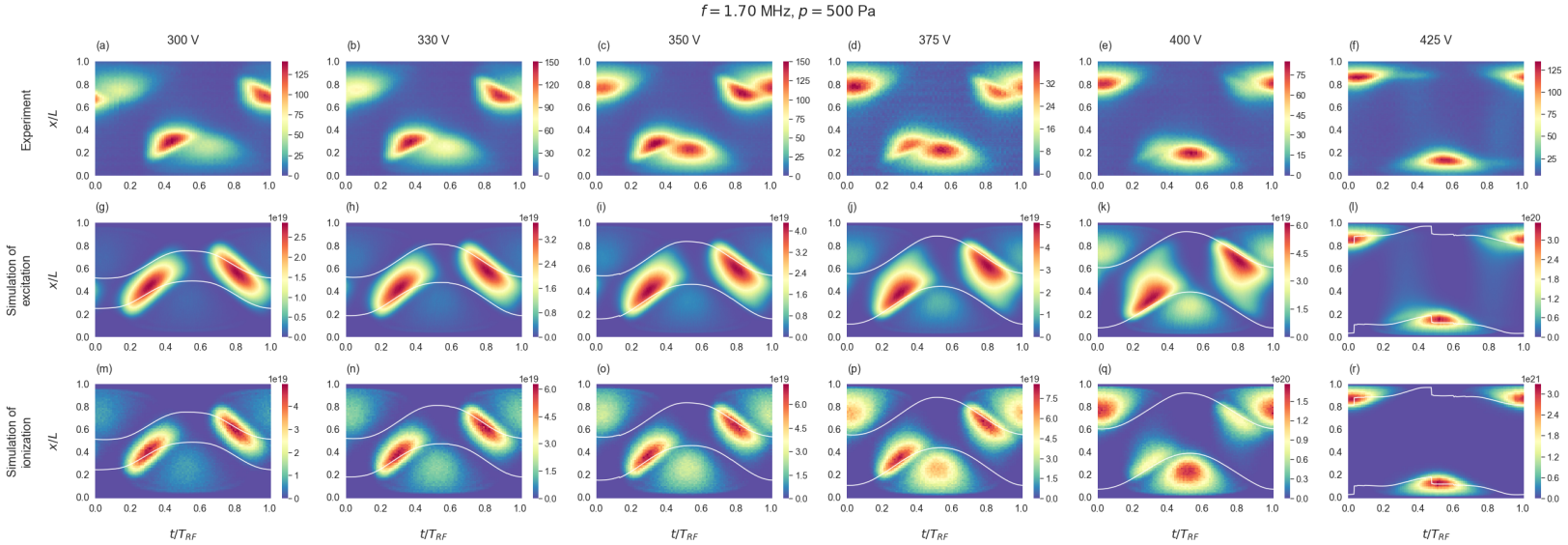

Figure 10: Spatio-temporal plots of the relative excitation rate of the Ne 2p1 state measured by PROES [a. u.] (a-f) and obtained from PIC/MCC simulation [a. u.] (g-l), and the ionization rate obtained from PIC/MCC simulation [$\mathrm{m^{-3}s^{-1}}$] (m-r). The sheath edges obtained from simulations are shown as white lines in panels (g-r). The powered electrode is located at $x/L = 0$, while the grounded electrode is at $x/L = 1$. Discharge conditions: $f = 1.70$ MHz, $L = 2.5$ cm, $p = 500$ Pa, the $V_{pp} = 2V_0$ peak-to-peak voltage varied between 300 V and 425 V.

intensive than the one obtained from PROES, however, a tendency of transition from α- to γ-mode can also be seen in this case. At the lowest peak-to-peak voltage value of 300 V, the PROES measurement shows an intensive α peak and a much less intensive but significant γ peak with approximately half of the intensity of the α peak for the excitation rate (10(a)), while this weaker γ peak is not remarkable in PIC/MCC simulation data for neither the excitation (10(g)) nor the ionization (10(m)). The experiment suggests a hybrid α-γ-mode with α being more significant, simulation suggests simple α-mode. The case is similar for 330 V, with the tendency of intensifying γ peak on PROES and simulated ionization data (10(b, m)). At 350 V, this tendency results in a γ peak in the experimentally observed excitation of similar intensity to the α peak (10(c)), forming hybrid α-γ-mode. The simulation still shows only weak γ-excitation (10(i)). At 375 V, PROES suggests the γ peak to be stronger than the α peak in the hybrid mode, while simulation only follows the intensifying tendency of the γ peak, even in the case of ionization. However, at 400 V, dominant γ-mode can be observed both in the case of the measured excitation and the simulated ionization (10(e, q)), but not in the case of the simulated excitation (10(k)). The experiment shows negligible α peak compared to γ at this high voltage (10(e)). Although PIC simulation suggests α-mode to be dominant based on the excitation (10(k)), it suggests dominant γ-mode and weaker α-mode in the ionization (10(q)). At the highest peak-to-peak voltage of 425 V studied here, all quantities, i.e. the measured and simulated excitation and the simulated ionization show pure γ-mode. To summarize shortly: at 1.70 MHz driving frequency and 500 Pa pressure, the ionization dynamics changes from α- to γ-mode as an effect of increasing the peak-to-peak voltage from 300 V to 425 V. However, PROES measurements of Ne 2p1 excitation and PIC/MCC simulations of Ne 2p1 excitation and ionization suggest the transition to happen at different values of the peak-to-peak voltage: the experiment suggests it to happen between 350 V and 375 V, PIC simulation suggests that the ionization changes from α- to γ-mode between 375 V and 400 V, while the characteristics of the spatio-temporal distribution of the simulated excitation

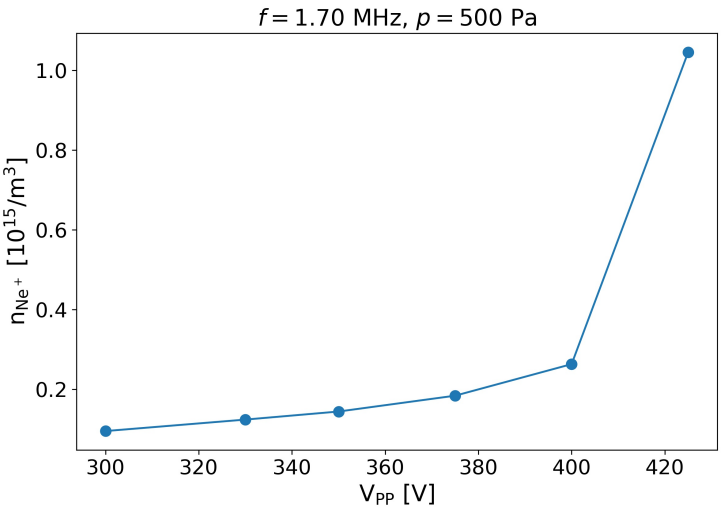

Figure 11: The peak ion densities as a function of the peak-to-peak voltage, for driving frequency of 1.70 MHz and pressure of 500 Pa.

show mode transition only between 400 V and 425 V.

Figure 11 shows the peak ion densities obtained by PIC/MCC simulations, i.e. the maximal density of Ne^+ ions in the discharge, for the discharge cases previously introduced in figure 10, as a function of the peak-to-peak voltage. As it can be seen in figure 11, the density increases as a function of the peak-to-peak voltage. This can be explained with the stronger acceleration of the electrons and the increasing ionization cross section as a function of the energy in the regime between ~ 20 eV and 200 eV (see figure 7). Note that for a certain peak-to-peak voltage, the maximal energy of electrons is the value of the voltage amplitude measured in eV, e.g. 200 eV in case of 400 V peak-to-peak voltage. With increasing the peak-to-peak voltage from 300 V to 400 V, the density increases by a factor of ~ 2.8. However, between 400 V and 425 V, the increase factor is ~ 4.0. As it is visible in figure 10, the sheath lengths drastically decrease when the peak-to-peak voltage is increased from 400 V to 425 V. At 425 V peak-to-peak voltage, the multiplication of γ-electrons in the sheaths become very efficient, which results in a higher ion density in the whole discharge cell and in the sheaths, decreasing

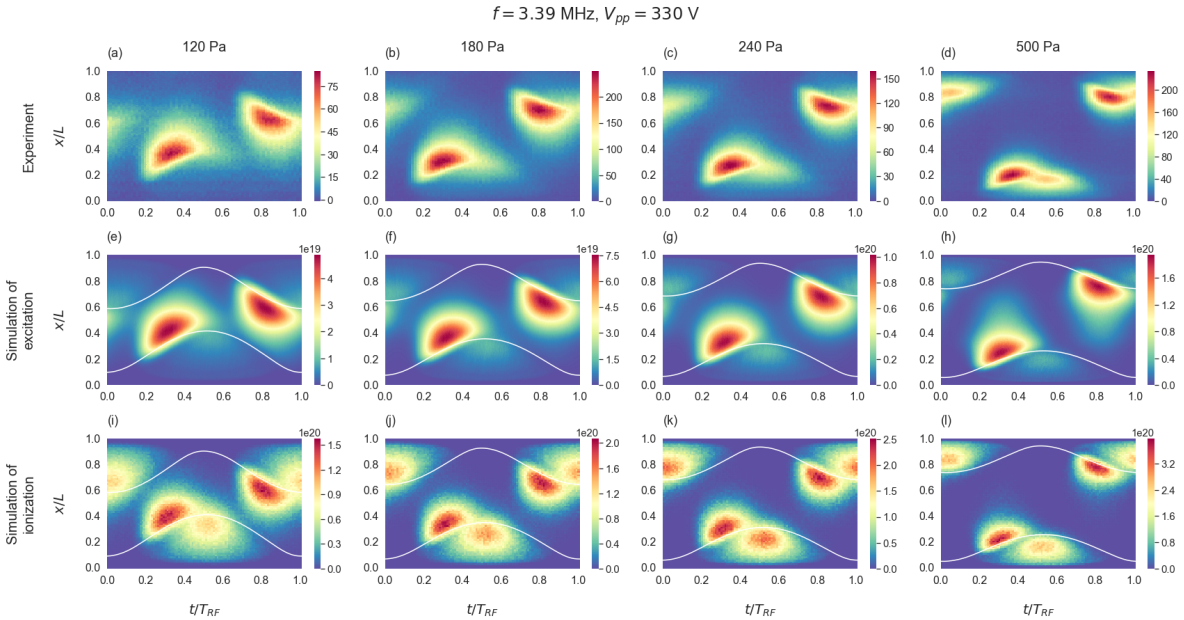

Figure 12: Spatio-temporal plots of the relative excitation rate of the Ne 2p1 state measured by PROES [a. u.] (a-d) and obtained from PIC/MCC simulation [a. u.] (e-h), and the ionization rate obtained from PIC/MCC simulation [$\mathrm{m^{-3}s^{-1}}$] (i-l). The sheath edges obtained from simulations are shown as white lines in panels (e-l). The powered electrode is located at $x/L = 0$, while the grounded electrode is at $x/L = 1$. Discharge conditions: $f = 3.39$ MHz, $L = 2.5$ cm, $V_{pp} = 2V_0 = 330$ V, the pressure varied between 120 Pa and 500 Pa.

the length of the latter and increasing the peak charge density. However, the cross section of ionization does not increase above 200 eV. Thus, this drastic increase of the γ-electron's multiplication as a consequence of changing the peak-to-peak voltage from 400 V to 425 V can only be explained by the next scenario: electrons born in γ-ionization and accelerated by the sheath potential suddenly overcome the ionization threshold, 22 eV, and cause an exponential multiplication.

3.2 Fixed peak-to-peak voltage

At the higher frequency of 3.39 MHz (figure 12), the peak-to-peak voltage is fixed at a lower level of 330 V, while the effect of changing the pressure is examined between 120 Pa and 500 Pa, corresponding to columns from left to right in the figure. First of all, the Ne 2p1 excitation rates measured by PROES (first line) and obtained from PIC/MCC simulations (second line) are in a good agreement at this frequency between 120 Pa and 240 Pa. The excitation rates suggest α-mode operation, and there is a weak γ patch that intensifies as the pressure is increased from 120 Pa to 240 Pa. This patch is slightly less intensive in the plots corresponding to simulation results (12(e-g)) compared to the ones that show experimental results (12(a-c)). However, at the highest pressure of 500 Pa, the measured and simulated excitation rate is remarkably different (12(d, h)). The PROES measurement suggests hybrid α-γ-mode with more significant α peak, while the excitation rate calculated by PIC/MCC simulation implies pure α mode. As for the ionization dynamics obtained by simulations (third row), hybrid α-γ-mode can be seen for all values of the pressure, and the γ peak slightly increases with increasing pressure (12(i-l)). The α-type ionization is more significant than γ in the whole pressure range. The fact that PROES measurements and PIC/MCC simulations provide similar results for the Ne 2p1 excitation rate between 120 Pa and 240 Pa suggests that the simulation reflects the ionization dynamics correctly in this regime. This is a typical example of the scenario when the observation of the Ne 2p1 excited state by PROES does not reflects the ionization dynamics correctly, as they have different spatio-temporal distribution. In the case of 500 Pa, in which the γ peak measured by PROES is remarkably more intensive than the one obtained by PIC/MCC simulation (12(d) compared to 12(h)), the simulation probably underestimates the role of γ-electrons, i.e. the γ-type ionization can be more significant than it can be seen in figure 12(l). With an ion-induced SEE coefficient higher than $\gamma = 0.2$, better agreement is expected at this relatively high pressure as well. The reason why the effect of the underestimation of SEE escalates at high pressure is that the multiplication of γ-electrons is less efficient at lower

pressures. In the case of longer electron free paths much less γ electrons collide with the atoms of the background gas within the sheaths. This has an effect on the sheath lengths as well: as the pressure is decreased, the sheaths get longer (see for example in figure 12, from panel (h) to (e) and (l) to (i)), as less ionization processes result in lower density near the electrodes. Another meaningful observation that can be made by examining the sheaths in figure 12 is the comparison of the sheath lengths obtained from simulation and PROES measurement. As in the case of the experimental data only the spatio-temporal distribution of the excitation is available (and no calculated curve for the boundary of the sheath), this is a comparison "by eye". For all values of the pressure, the sheaths seem to be systematically shorter according to PROES than the ones calculated by PIC/MCC simulation (the experimentally measured excitation peaks are closer to the electrodes than the ones obtained from simulations). This is another indication that the simulation underestimates the role of γ-electrons, i.e. a SEE coefficient higher than 0.2 would be more realistic.

Figure 13 shows a study of the effect of the pressure on the discharge characteristics at the frequency of 6.78 MHz, the value of the peak-to-peak voltage being 330 V, the same as in the previous case (3.39 MHz). The structure of the figure is identical to figure 12, however, the pressure has a wider range here, starting with 60 Pa and increasing to 500 Pa. At this higher frequency, the excitation rate of the Ne 2p1 state obtained from PROES measurements (first row) and PIC/MCC simulation (second row) tend to be closer to each other than in the previous cases. Between 60 Pa and 240 Pa, the excitation rates are in a good agreement (see figure 13(a-c) in comparison with 13(e-g)). The spatio-temporal distributions of the excitation suggest α mode, the sheath lengths decrease as a function of the pressure, and a γ patch slightly intensifies at each electrode (see for example in panel 13(c) around $t/T_{RF} = 0.5$, at the powered electrode, i.e. the bottom of the figure). However, the sheath lengths seem to be shorter according to the experiment than based on the simulation for this frequency as well, and the γ patch is weaker in the spatio-temporal distribution obtained from simulation than in the one

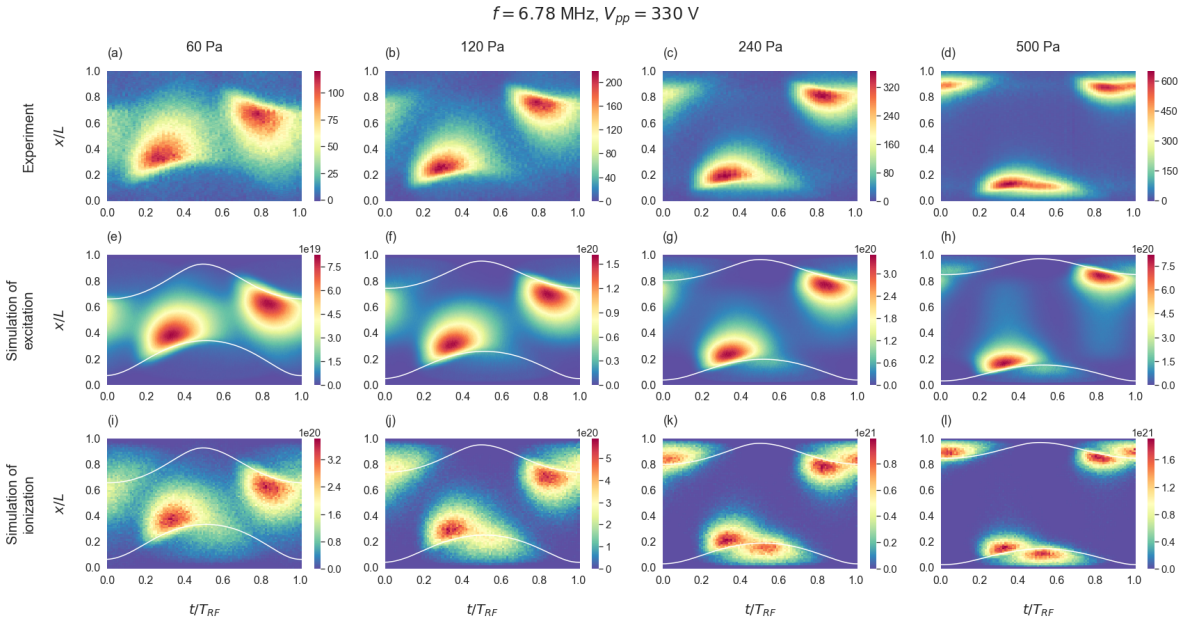

Figure 13: Spatio-temporal plots of the relative excitation rate of the Ne 2p1 state measured by PROES [a. u.] (a-d) and obtained from PIC/MCC simulation [a. u.] (e-h), and the ionization rate obtained from PIC/MCC simulation [$\mathrm{m^{-3}s^{-1}}$] (i-l). The sheath edges obtained from simulations are shown as white lines in panels (e-l). The powered electrode is located at $x/L = 0$, while the grounded electrode is at $x/L = 1$. Discharge conditions: $f = 6.78$ MHz, $L = 2.5$ cm, $V_{pp} = 2V_0 = 330$ V, the pressure varied between 60 Pa and 500 Pa.

measured by PROES. This implies again that the secondary electron emission may be underestimated. At the highest pressure of 500 Pa, PROES suggests hybridα-γ-mode 13(d), while the excitation rate obtained by PIC/MCC simulation shows pure α-mode 13(h). Similarly to the case of 3.39 MHz, the effect of the underestimation of γ escalates at this relatively high pressure of 500 Pa. Regarding the ionization rates obtained from PIC/MCC simulations (third row), a γ peak is visible at each electrode for all values of the pressure, even when it is not suggested by the excitation rate. This γ peak significantly intensifies as the pressure is increased, i.e. a transition from α-mode to α-γ hybrid mode can be observed regarding the ionization dynamics of the discharge,

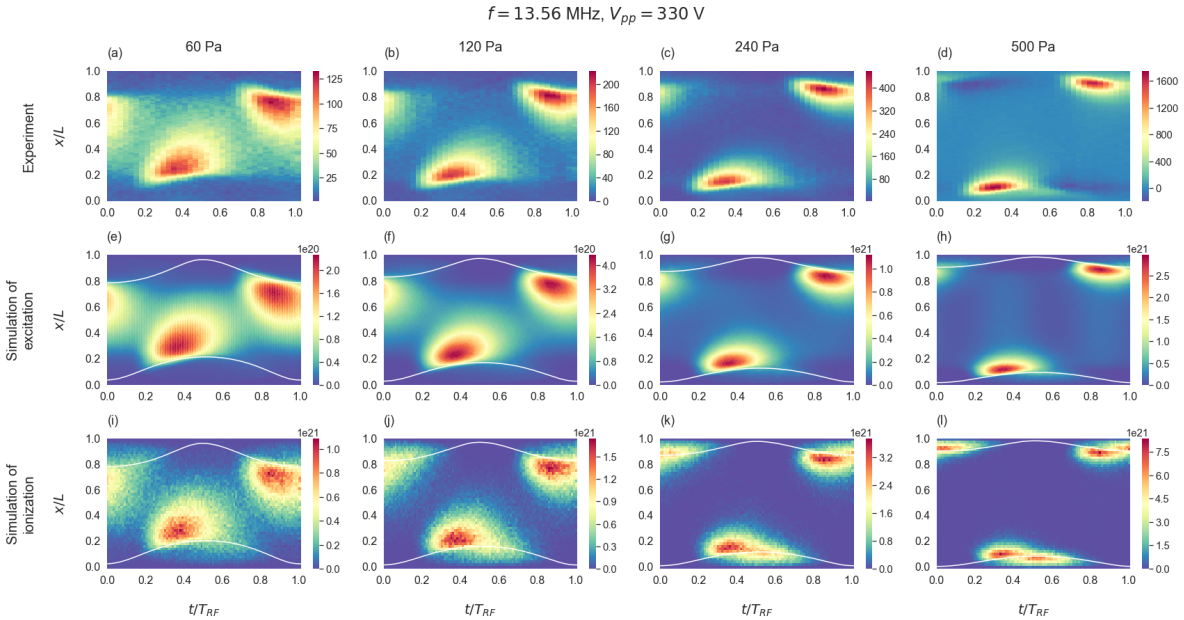

Figure 14: Spatio-temporal plots of the relative excitation rate of the Ne 2p1 state measured by PROES [a. u.] (a-d) and obtained from PIC/MCC simulation [a. u.] (e-h), and the ionization rate obtained from PIC/MCC simulation [$\mathrm{m^{-3}s^{-1}}$] (i-l). The sheath edges obtained from simulations are shown as white lines in panels (e-l). The powered electrode is located at $x/L = 0$, while the grounded electrode is at $x/L = 1$. Discharge conditions: $f = 13.56$ MHz, $L = 2.5$ cm, $V_{pp} = 2V_0 = 330$ V, the pressure varied between 60 Pa and 500 Pa.

as the pressure is increased from 60 Pa to 500 Pa 13(i-l). Based on the fact that the underestimation of SEE in PIC/MCC simulations results in a remarkably different spatio-temporal distribution of the excitation rate from the one obtained by PROES measurement at 500 Pa, γ-mode is probably even more dominant in the ionization than it can be seen in figure 13(l). It can also be seen that PROES measurement does not probe the ionization dynamics correctly, since the γ peaks that are present in the spatio-temporal distribution of the ionization obtained by PIC/MCC simulation are much weaker in the excitation rate measured by PROES, sometimes being hardly visible in it.

The highest frequency studied in this work is 13.56 MHz. Discharges are examined in the same pressure regime and the same peak-to-peak voltage of 330 V as in the case of 6.78 MHz. The results are presented in figure 14. At this relatively high frequency, the spatio-temporal distribution of the Ne 2p1 excitation rate obtained from PROES measurements (first row) and PIC/MCC simulations (second row) are in clear agreement for all values of the pressure between 60 Pa and 500 Pa. In addition, the sheath lengths obtained by PIC/MCC simulations are also very close to the ones suggested by PROES measurements. No significant difference is observable between the results of the experiments and the simulations in case of any of the pressure values examined here. This implies that for driving frequency of 13.56 MHz and peak-to-peak voltage of 330 V, within the pressure range from 60 Pa to 500 Pa, the PIC/MCC simulation method applied in this work describes the discharge correctly. The use of a constant ion-induced SEE coefficient with value of $\gamma = 0.2$ does not seem to be an underestimation. At the lowest pressures of 60 Pa and 120 Pa, the spatio-temporal distributions of the ionization rates obtained from PIC/MCC simulations do not differ remarkably from the distribution of the Ne 2p1 excitation (see 14(i) compared to 14(a, e) and 14(j) compared to 14(b, f)). Both suggests α-mode, however, a weak γ-patch can be seen within the sheaths in the ionization patterns. At 240 Pa, the spatio-temporal distribution of the simulated ionization becomes significantly different from the excitation rates obtained by PROES measurement and PIC/MCC simulation. The ionization starts to operate in hybrid α-γ-mode, in which the α peak is more intensive (14(k)). As for the excitation, though, both the experiment and the simulation implies α-mode (14(c, g)). At the highest pressure of 500 Pa, the PIC/MCC simulation exhibits hybrid α-γ-mode for the ionization dynamics (14(l)), while the spatio-temporal distribution of the Ne 2p1 excitation is dominated by α-mode both in case of PROES measurement and PIC/MCC simulation (14(d, h)). To tell it shortly, a transition from α to α-γ hybrid mode can be observed in the ionization dynamics of a neon discharge operated at driving frequency of 13.56 MHz and peak-to-peak voltage of 330 V as the pressure is increased from 60 Pa

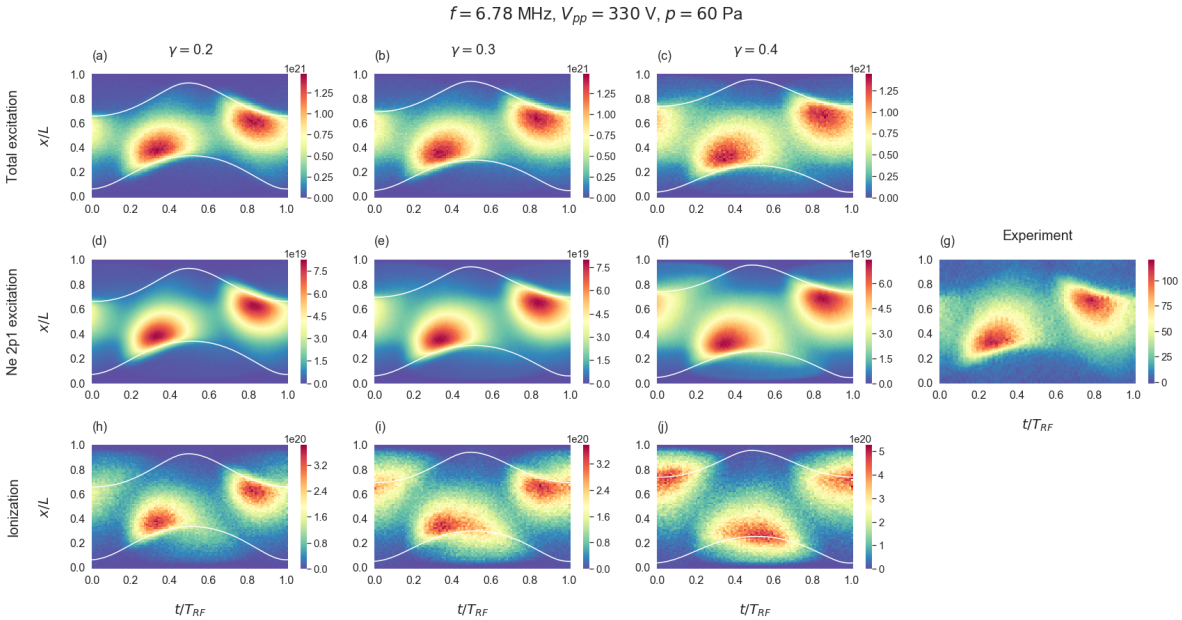

Figure 15: Spatio-temporal plots of the total excitation rate [$m^{-3}s^{-1}$] (a-c), the relative excitation rate of the Ne 2p1 state [a. u.] (d-f) and the ionization rate [$m^{-3}s^{-1}$] (h-j) obtained from PIC/MCC simulation, considering different coefficients for the ion-induced secondary electron emission: $\gamma = 0.2$ (1^{st} column from left), 0.3 (2^{nd} column) and 0.4 (3^{rd} column). The sheath edges obtained from simulations are shown as white lines in panels (a-f) and (h-j). Panel (g) shows the Ne 2p1 excitation rate measured by PROES [a. u.]. The powered electrode is located at $x/L = 0$, while the grounded electrode is at $x/L = 1$. Discharge conditions: $f = 6.78$ MHz, $L = 2.5$ cm, $V_{pp} = 2V_0 = 330$ V, $p = 60$ Pa.

to 500 Pa. However, this transition cannot be seen in the spatio-temporal distribution of the excitation, i.e. it cannot be observed by PROES.

3.3 Variation of γ

After introducing experimental and simulation results for neon RF discharges operated in a wide parameter regime, the influence of the choice of the γ ion induced secondary

electron emission (SEE) coefficient on the excitation and ionization dynamics is examined. In all the simulations introduced above, the γ coefficient was set to 0.2. For driving frequencies of 3.39 MHz and above and pressures up to 240 Pa, at peak-to-peak voltage of 330 V, PIC/MCC simulation produced results in good agreement with PROES. The differences decreased with increasing frequency and increased with increasing pressure. In case of 500 Pa, the PIC/MCC simulation was found to underestimate the SEE caused by ions and consequently to underestimate the role of γ-electrons in the ionization dynamics. At driving frequency of 1.70 MHz, the underestimation of SEE was also found. In the following, PIC/MCC simulation results are presented obtained by assuming higher values for the γ SEE coefficient. In figure 15 and 16, the results obtained for driving frequency of 6.78 MHz, peak-to-peak voltage of 330 V and pressure values of 60 Pa and 500 Pa, by assuming $\gamma = 0.2$, are compared to simulation results for the same conditions with γ coefficients of 0.3 and 0.4. The first three columns in these figures correspond to a certain value of the gamma, while panel (g) at the right edge shows the experimentally measured Ne 2p1 excitation rate for the studied discharge conditions. The rows correspond to the simulated total excitation rate, the Ne 2p1 excitation rate and the ionization rate. The total excitation rate means the number of electron-atom excitation processes that occur in the discharge per unit time per unit volume, i.e. it contains all kinds of excitation, not only 2p1.

Figure 15 shows the results for 60 Pa, the lowest pressure value studied at the frequency of 6.78 MHz. It can be seen in the first two lines that the spatio-temporal distribution of the total excitation and the Ne 2p1 excitation rate is very similar for a certain PIC/MCC simulation (one column of the figure). As a function of γ, the excitation does not changes remarkably. The sheath lengths slightly decrease as the γ coefficient is increased (15(a-c, d-f)), as a consequence of the multiplication of the γ-electrons. The PROES measurement produces fairly similar Ne 2p1 excitation rate to the ones obtained from PIC/MCC simulations, for all the γ values studied here (15(g)). However, γ-type ionization gets significant for higher values of the SEE coefficient, i.e.

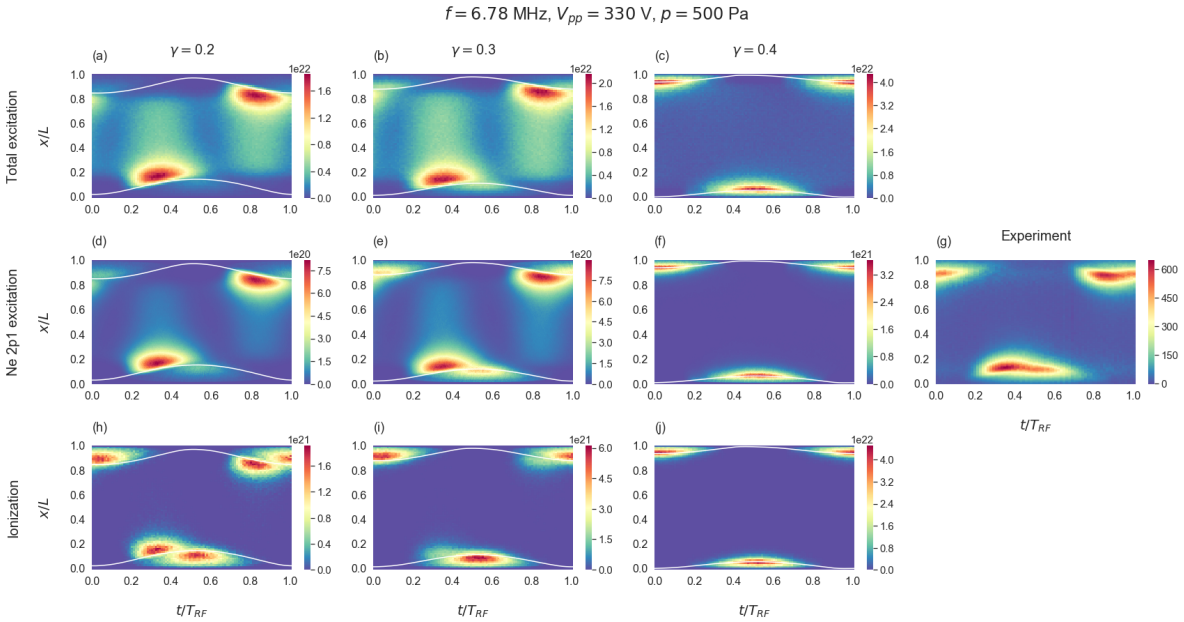

Figure 16: Spatio-temporal plots of the total excitation rate [$m^{-3}s^{-1}$] (a-c), the relative excitation rate of the Ne 2p1 state [a. u.] (d-f) and the ionization rate [$m^{-3}s^{-1}$] (h-j) obtained from PIC/MCC simulation, considering different coefficients for the ion-induced secondary electron emission: $\gamma = 0.2$ (1^{st} column from left), 0.3 (2^{nd} column) and 0.4 (3^{rd} column). The sheath edges obtained from simulations are shown as white lines in panels (a-f) and (h-j). Panel (g) shows the Ne 2p1 excitation rate measured by PROES [a. u.]. The powered electrode is located at $x/L = 0$, while the grounded electrode is at $x/L = 1$. Discharge conditions: $f = 6.78$ MHz, $L = 2.5$ cm, $V_{pp} = 2V_0 = 330$ V, $p = 500$ Pa.

$\gamma = 0.3$ and 0.4 (15(h-j)). While for $\gamma = 0.2$, the ionization operates in α-mode, for $\gamma = 0.4$ most of the ionization processes happen at the phase of sheath expansion. The latter one is called γ-mode, however, in this case, the γ ionization peak does not escalates within the sheath but further from the electrode. The reason is the low value of the pressure, which causes a mean free path for electrons of approximately the maximal length of the sheath.

Figure 16 shows the effects of the choice of the γ ion-induced SEE coefficient on the

discharge characteristics at 6.78 MHz frequency, 330 V peak-to-peak voltage and 500 Pa, the pressure at which the assumption of $\gamma = 0.2$ was found to be an underestimation. In case of $\gamma = 0.2$ coefficient, the ionization operates in a hybrid α-γ-mode, as it was presented earlier in figure 13(l) and can be seen here in panel 16(h). The simulation of excitation suggests α-mode to be dominant (16(a, d)), however, PROES measurement shows hybrid α-γ-mode (16(g)). The spatio-temporal distribution of the total excitation and the Ne 2p1 excitation obtained from PIC/MCC simulation is similar. As increasing the value of the SEE coefficient, a mode transition can be observed, i.e. the value of γ is critical in terms of the discharge operation. At $\gamma = 0.3$, γ-mode dominates the ionization dynamics instead of the balanced hybrid α-γ-mode observed in case of $\gamma = 0.2$ (16(i) in comparison with 16(h)). Meanwhile the excitation suggests hybrid α-γ-mode instead of the dominant α-mode (16(e) in comparison with 16(d)). For the largest γ value of 0.4, a pure γ-mode can be observed in the spatio-temporal distributions of the ionization dynamics (16(j)), which can also be seen in the case of the total excitation rate (16(c)) and the Ne 2p1 excitation rate (16(f)). Another important remark concerning the current set of simulations with different γ coefficients is that the simulation results for the Ne 2p1 excitation rate obtained with the assumption of different γ values can be compared to the result of PROES measurement, providing a verification for the simulation. As it can be seen, under the conditions of 6.78 MHz, 330 V and 500 Pa, among the cases investigated here, $\gamma = 0.3$ provides the best agreement with the experiment.

As a final remark, the peak charge densities obtained from PIC/MCC simulations are shown in figure 17 as a function of the pressure, for most of the discharge cases studied above, at peak-to-peak voltage of 330 V and driving frequencies of 3.39 MHz, 6.78 MHz and 13.56 MHz. At a fixed frequency, the peak charge density increases as a function of the pressure, as a result of more frequent collisions due to shorter electron free path. At a certain pressure, the peak charge density also increases as the driving frequency is increased, and this difference in the density between discharges operated

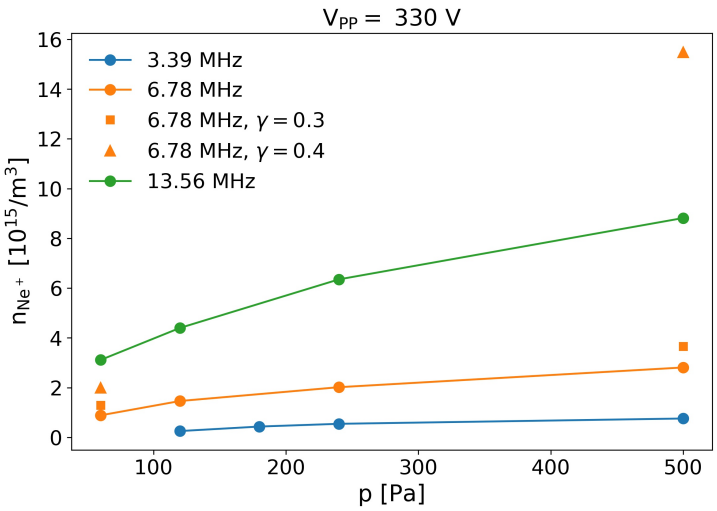

Figure 17: The peak ion densities as a function of the pressure at 330 V peak-to-peak voltage, for different values of the driving frequency and the γ SEE coefficient. $\gamma = 0.2$ in the cases where it is not specified.

at different driving frequencies is more pronounced at higher pressures. For example, by changing the frequency from 3.39 MHz to 13.56 MHz, the density increases by a factor of ∼5 at 120 Pa, while it increases by a factor of ∼8 at 500 Pa. The choice of the SEE coefficient, γ is also critical in terms of the ion density. At 6.78 MHz and 60 Pa, the density increases by a factor of ∼2, as a result of applying $\gamma = 0.4$ SEE coefficient instead of 0.2. However, at 500 Pa, the density increases by a factor of ∼8 as the SEE coefficient is changed from 0.2 to 0.4. It is notable that a γ value of 0.3 results in much less impact on the density in comparison with 0.4, i.e. at 500 Pa, $\gamma = 0.3$ results in a 30 % higher density the value can be obtained in the case of $\gamma = 0.2$. This implies that the multiplication of the γ electrons become critical in the sheath when they are generated with a high probability of 40 %.

4 Conclusions

Within the frame of this work, the electron power absorption modes of low-pressure RF discharges operated in neon gas were studied, and a detailed comparison of simulated and experimental results was provided in a wide parameter regime. 1d3v Particle-in-Cell/Monte Carlo Collisions simulations and Phase Resolved Optical Emission Spectroscopy measurements were performed at driving frequencies from 1.70 MHz to 13.56 MHz, pressures from 60 Pa to 500 Pa and peak-to-peak voltages from 300 V to 425 V in a geometrically symmetric CCP reactor.

Both in simulations and experiments, a transition of the discharge operation mode from α to γ was found by increasing the peak-to-peak voltage at a fixed frequency of 1.70 MHz and a fixed pressure of 500 Pa. However, the simulations and the experiments suggested different peak-to-peak voltages at which the transition happened. Surprisingly, PROES measurements shown more intensive γ-peaks in the spatio-temporal distribution of the Ne 2p1 excitation than PIC/MCC simulations did in the spatio-temporal ionization rate. This observation implied that the use of a constant γ value of 0.2 as ion-induced secondary electron emission coefficient is an underestimation of the role of γ-electrons at this low frequency.

Discharge operation mode transitions were also observed by increasing the pressure at fixed frequencies of 3.39 MHz, 6.78 MHz and 13.56 MHz, at a fixed peak-to-peak voltage of 330 V. In these cases, the Ne 2p1 excitation rates obtained from PROES measurements and PIC/MCC simulations shown a good agreement between pressures of 60 Pa and 240 Pa. However, it was revealed that significant γ-mode ionization could took place in the discharge even in the cases when it was not suggested by the spatio-temporal distribution of the Ne 2p1 excitation. At the relatively high pressure of 500 Pa, the underestimation of the secondary electron emission caused by ions resulted in remarkable differences between the spatio-temporal excitation rate obtained from PIC/MCC simulation and the excitation rate obtained from PROES measure-

ment, and in the underestimation of the γ-mode ionization. Via the comparison of experimental and simulated data within a wide parameter regime, this study also revealed the limitations of PROES to probe the discharge operation mode, which was determined by the ionization dynamics.

As another point, the critical role of the secondary electron emission coefficient assumed in the PIC/MCC simulation was studied briefly. It was found that for a relatively high pressure of 500 Pa, a γ coefficient above 0.2 results in better agreement of the excitation rate obtained by PIC/MCC simulation with the excitation rate measured by PROES. Together with this observation, the fact that simulation results show weaker ionization at the low frequency of 1.70 MHz compared to what is suggested by PROES measurements designates the topic of future investigations: the effect of ion-induced γ-electrons has to be considered more accurately in PIC/MCC simulations of neon discharges operated between stainless steel electrodes within the current parameter regime. On the other hand, the comparison of the excitation rate obtained from PIC/MCC simulation to the result of PROES measurement, for several simulation cases that assume different constant values for the γ SEE coefficient, can be used as a method to measure secondary electron emission coefficients of a certain system. This type of measurement is called γ-cust, and it has only been applied for argon gas [19].

5 Acknowledgements

This work would not have been possible without the help and support of many people. I would like to say thank you to all of them.

- First of all, to Aranka Derzsi, my supervisor, for providing the opportunity to work with her, for supporting my visit to conferences, for all our discussions, her instructions and ideas, and for being patient and helpful.
- To Zoltán Donkó, who was my first teacher in plasma Physics, invited me to join the Electrical Gas Discharges research group in Wigner Research Centre for Physics at the Hungarian Academy of Sciences, and helped a lot with his ideas.
- To Péter Hartmann, for coordinating the measurements, answering my questions thoroughly, and for maintainance of the *plasma* cluster.
- To Ihor Korolov, for coordinating the measurements and answering my questions thoroughly.
- To Julian Schulze, for supporting my visit to conferences, for providing the ICCD camera for the measurements, and for the discussions.
- To Kinga Kutasi, head of the research group, for allowing me to work for the Electrical Gas Discharges research group.
- To Ákos Horváth, my supervisor on behalf of Eötvös University.

This work was supported by the US NSF grant no. PHY. 1601080, by the DFG (SFB-TR 87 project C1), and Hungarian grants K-119357 and PD-121033 and FK-128924.

References

[1] M A Lieberman and A J Lichtenberg: Principles of Plasma Discharges and Materials Processing (Wiley-Interscience, New York, 2005)

[2] Z Donkó: Alacsony hőmérsékletű plazmafizika. Lecture notes, 2018

[3] J Schulze, A Derzsi, K Dittmann, T Hemke, J Meichsner and Z Donkó 2011 *Phys. Rev. Lett.* **107** 275001

[4] J Schulze, Z Donkó, D Luggenhölscher and U Czarnetzki 2009 *Plasma Sources Sci. Technol.* **18** 034011

[5] C K Birdsall 1991 *IEEE Trans. Plasma Sci.* **19** 65

[6] Z Donkó, J Schulze, U Czarnetzki, A Derzsi, P Hartmann, I Korolov, E Schuengel 2012 *Plasma Phys. Control. Fusion* **54** 124003

[7] J P Verboncoeur 2005 *Plasma Phys. Control. Fusion* **47** A231

[8] K Matyash, R Schneider, F Taccogna, A Hatayama, S Longo, M Capitelli, D Tskhakaya and F X Bronold 2007 *Contrib. Plasma Phys.* **47** 595

[9] D Tskhakaya, K Matyash, R Schneider and F Taccogna 2007 *Contrib. Plasma Phys.* **47** 563

[10] B Horváth: Rádiófrekvenciás gerjesztésű gázkisülések numerikus szimulációja. Bachelor thesis, Eötvös Loránd University, Budapest, 2017

[11] Kollath R: Encyclopedia of Physics Vol. XXI, ed. Flügge S (Berlin, Springer, 1956), p 264

[12] Z Donkó 2011 *Plasma Sources Sci. Technol.* **20** 24001

[13] SIGLO database, `www.lxcat.net`, retrieved on January 4, 2019.

[14] Biagi-v7.1 database, www.lxcat.net, retrieved on January 23, 2019.
Cross sections extracted from PROGRAM MAGBOLTZ, VERSION 7.1 JUNE 2004.

[15] J Schulze, E Schüngel, Z Donkó, D Luggenhölscher and U Czarnetzki 2010 *J. Phys. D: Appl. Phys.* **43** 124016

[16] https://www.nist.gov/pml/atomic-spectra-database

[17] J E Chilton, M D Stewart and C C Lin 2000 *Phys. Rev. A* **61** 52708

[18] R P Brinkmann 2007 *J. Appl. Phys.* **102** 093303

[19] M Daksha, B Berger, E Schüngel, I Korolov, A Derzsi, M Koepke, Z Donkó and J Schulze 2016 *J. Physics D: Applied Physics* **49** 234001